

## Article

# Simple Preparation and Characterization of Hierarchical Flower-like NiCo<sub>2</sub>O<sub>4</sub> Nanoplates: Applications for Sunset Yellow Electrochemical Analysis

Hadi Beitollahi <sup>1,\*</sup> , Somayeh Tajik <sup>2</sup>, Zahra Dourandish <sup>1</sup> and Fariba Garkani Nejad <sup>1</sup>

<sup>1</sup> Environment Department, Institute of Science and High Technology and Environmental Sciences, Graduate University of Advanced Technology, Kerman P.O. Box 76318-85356, Iran

<sup>2</sup> Research Center of Tropical and Infectious Diseases, Kerman University of Medical Sciences, Kerman P.O. Box 76169-13555, Iran

\* Correspondence: h.beitollahi@yahoo.com

**Abstract:** The current work was performed to construct a novel electrochemical sensing system for determination of sunset yellow via the modification of screen-printed graphite electrode modified with hierarchical flower-like NiCo<sub>2</sub>O<sub>4</sub> nanoplates (NiCo<sub>2</sub>O<sub>4</sub>/SPGE). The prepared material (hierarchical flower-like NiCo<sub>2</sub>O<sub>4</sub> nanoplates) was analyzed by diverse microscopic and spectroscopic approaches for the crystallinity, composition, and morphology. Chronoamperometry, differential pulse voltammetry, linear sweep voltammetry, and cyclic voltammetry were used for determination of the electrochemical behavior of sunset yellow. The as-fabricated sensor had appreciable electro-catalytic performance and current sensitivity in detecting the sunset yellow. There were some advantages for NiCo<sub>2</sub>O<sub>4</sub>/SPGE under the optimized circumstances of sunset yellow determination, including a broad dynamic linear between 0.02 and 145.0 μM, high sensitivity of 0.67 μA/(μM.cm<sup>2</sup>), and a narrow limit of detection of 0.008 μM. The practical applicability of the proposed sensor was verified by determining the sunset yellow in real matrices, with satisfactory recoveries.

**Keywords:** sunset yellow; flower-like NiCo<sub>2</sub>O<sub>4</sub> nanoplates; voltammetry; modified electrode



**Citation:** Beitollahi, H.; Tajik, S.; Dourandish, Z.; Garkani Nejad, F. Simple Preparation and Characterization of Hierarchical Flower-like NiCo<sub>2</sub>O<sub>4</sub> Nanoplates: Applications for Sunset Yellow Electrochemical Analysis. *Biosensors* **2022**, *12*, 912. <https://doi.org/10.3390/bios12110912>

Received: 8 September 2022

Accepted: 14 October 2022

Published: 22 October 2022

**Publisher's Note:** MDPI stays neutral with regard to jurisdictional claims in published maps and institutional affiliations.



**Copyright:** © 2022 by the authors. Licensee MDPI, Basel, Switzerland. This article is an open access article distributed under the terms and conditions of the Creative Commons Attribution (CC BY) license (<https://creativecommons.org/licenses/by/4.0/>).

## 1. Introduction

Food additives applied in processed foodstuff can normally improve some features such as flavor, appearance, color, taste, nutritive value, preservation, and texture [1]. Color has always encouraged consumers to buy a food product, usually because of the mere fact that it is visual at the first sight. A buyer can be affected negatively or positively by colors. In the food industry, natural dyes in food products can be intensified or preserved using food dyes. The pharmaceutical industry also exploits edible coloring to create a different look in their products. The edible colors can be natural or synthetic. Natural dyes originate from animal or plant sources, by extraction through physical techniques such as riboflavin. The natural color of the edible products may be lost during various stages including heating, processing, storage, and distribution. Synthetic dyes are composed of artificially synthesized organic and inorganic compounds. Among these, a special place in food industry has been established for the synthetic colorants as good alternatives to natural dyes because of appreciable merits such as long-lasting stability, easy coloring, minimal microbiological and chemical or physical contamination [2,3]. Azo dyes with a broad spectrum of colors owing to a unique chemical structure account for about 65% of the commercial dye market around the world [4,5]. Disodium 2-hydroxy-1-(4-sulphonatophenylazo) naphthalene-6-sulphonate, or sunset yellow, as a widely used synthetic azo dye can be found in various beverages, foods, medicines, colorings, and cosmetics, which is cost-effective with stable structure and bright color [6–8]. The allowance limit of sunset yellow as food additive must be <50 ppm [9]. Hence, doses exceeding this limit can be associated with complications

such as kidney failures, attention deficit hyperactivity disorder (ADHD), hepatocellular damage, cancers, and headache [10,11]. Accordingly, there have been various analytical approaches for sensing and quantifying the sunset yellow in food matrices, some of which are coupling ionic liquid-based aqueous two-phase systems (IL-ATPSs) with high performance liquid chromatography (HPLC) [12], reversed-phase ion pair high-performance liquid chromatography [13], spectrophotometry [14], HPLC/mass spectrometry (HPLC-MS) [15], ion-pair liquid chromatography with on-line photodiode-array and electrospray mass spectrometry [16], capillary electrophoresis [17], and high-performance thin-layer chromatographic combined with image processing of scanned chromatograms [18]. However, their use is often limited due to reasons such as being expensive, time-consuming, or requiring tedious pretreatment.

Among these, electrochemical analysis has had special place in determining the bioactive molecules, nutrients, drugs, contaminants, and food additives owing to cost-effectiveness, facile use, rapidity, high sensitivity and selectivity [19–33], thereby making them a good alternative to the above-mentioned techniques. There are several conventional solids (such as glassy carbon, carbon paste, and gold) or disposable electrodes (such as screen-printed electrodes or SPEs) to construct the electrochemical sensors. Special attention in the field of electroanalytical research has recently been drawn to SPEs in the manufacture of (bio) sensors. The SPEs are appropriate electrochemical transducers because of high sensitivity, ease of use, and cost-effective properties when comparing with conventional diagnostics [34–38]. Such devices possess a miniaturized system consisting of the working, auxiliary, and reference electrodes. Hence, there is a need for the small volume of solution for electrochemical determination, which is indeed interesting in terms of green chemistry [39,40]. Chemically modified electrodes (CMEs) are the result of the intentional fixation of a modifying agent on the surface of electrode by various physical and chemical methods [41,42]. Many studies have shown that improvements in the sensitivity and selectivity of electrochemical sensors are achieved due to modifications of the electrode surface [43,44]. Nanomaterial-supported electrochemical sensing systems have been considered by many researchers due to their capability for carrying out the electrochemical analysis of diverse analytes [45]. The electrode surface modification using diverse nanostructures can enhance the analyte-specific electrochemical reactivity and sensitivity [46,47].

Nanomaterials and their applications in various fields have become a distinct and active area of scientific and technological developments over the recent years [48–56]. In this regard, the metal oxide nanoparticles are applied extensively in some fields such as energy production, food technology and preservative, medicine, catalysis and electrocatalysis because of intrinsic redox features and morphological and structural flexibility [57–61]. One of the best electrode modifiers is binary transition-metal oxide because of superior resistance to deactivation, appreciable selectivity, and high catalytic performance [62,63]; for example,  $\text{NiCo}_2\text{O}_4$  nanostructures are mixed-metal oxides successful for sensors owing to electrochemical catalytic performance, high biocompatibility, commendable electronic conductivity, non-toxicity, and low cost.  $\text{NiCo}_2\text{O}_4$  has greater electronic conductivity and electrochemical performance when comparing with cobalt and nickel oxides. The synergic impact of nickel and cobalt elements in  $\text{NiCo}_2\text{O}_4$  provides a richer diversity of redox reactions when comparing with the monometallic  $\text{NiO}$  and  $\text{Co}_3\text{O}_4$  [64–66]. Accordingly,  $\text{NiCo}_2\text{O}_4$  is considered as an electrochemical material but still suffers from some problems with improvement in a small surface area, pore size, and intrinsically poor electro-conductivity [67]. Such bottlenecks can be circumvented by using materials based on two-dimensional or sheet-like morphology owing to the merits associated with large pore size, high surface area, short paths, and fast reaction kinetics for redox process [68,69]. Thus, 2D or sheet-like  $\text{NiCo}_2\text{O}_4$  can serve as an electrode material for the fabrication of electrochemical sensors.

The current work was performed to fabricate hierarchical flower-like  $\text{NiCo}_2\text{O}_4$  nanoplates by a facile method and to characterize their structure and morphology by diverse techniques.

Then, the as-produced nanoplates were used to modify the SPGE surface to construct a new sunset yellow sensor ( $\text{NiCo}_2\text{O}_4/\text{SPGE}$ ). The resulting modified electrode ( $\text{NiCo}_2\text{O}_4/\text{SPGE}$ ) had a great sensitivity towards the sunset yellow, possessing a narrow limit of detection (LOD) and a broad linear range. The analytical performance and practical applicability of proposed sensor was determined by sensing sunset yellow in real food specimens.

## 2. Experimental

### 2.1. Equipments

A Metrohm Autolab PGSTAT 320N Potentiostat/Galvanostat Analyzer (Herisau, Switzerland) with GPES (General Purpose Electrochemical System-version 4.9) software was applied for all electrochemical determinations at ambient temperature. Cyclic voltammetry (CV), Chronoamperometry (CA), differential pulse voltammetry (DPV) and linear sweep voltammetry (LSV) were employed to characterize the electro-analytical performance of the modified electrode toward sunset yellow. The electrochemical sensors were prepared by DRP-110 SPEs (DropSens, Oviedo, Spain) including a silver pseudo-reference electrode, graphite working electrode, and graphite auxiliary electrode. A Metrohm 713 pH-meter with glass electrode (Metrohm AG, Herisau, Switzerland) was used to determine and adjust the pH of the solution.

A Panalytical X'Pert Pro X-ray diffractometer (Almelo, The Netherlands) applying a  $\text{Cu}/\text{K}\alpha$  radiation ( $\lambda:1.54 \text{ \AA}$ ) was used for X-ray diffraction (XRD) analysis and a Bruker Tensor II spectrometer (Bruker, Karlsruhe, Germany) was employed to capture the Fourier transform-infrared (FT-IR) spectra. A MIRA3 scanning electron microscope (Tescan, Brno, Czech Republic) coupled with an X-ray spectroscopy (EDS) detector was utilized for field emission-scanning electron microscopy (FE-SEM) images and elemental analysis.

### 2.2. Solvents and Chemicals

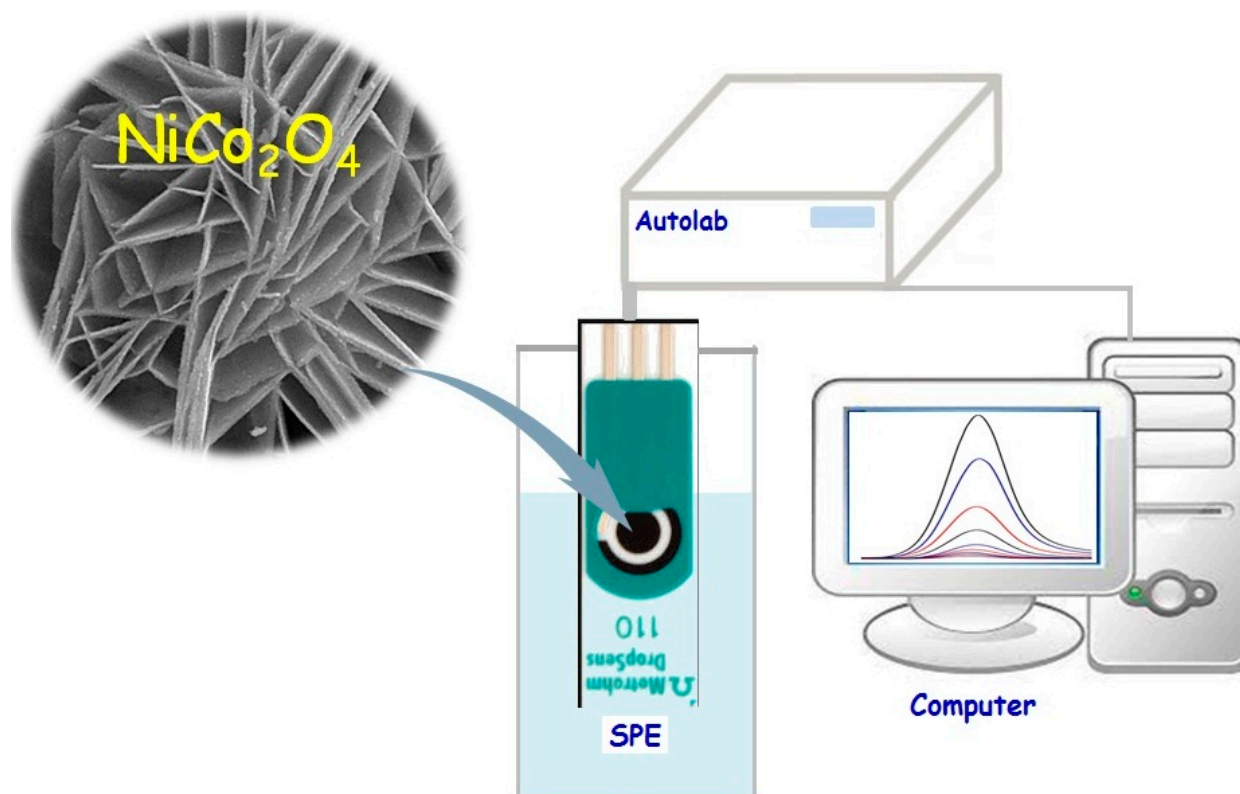
All solvents and chemicals applied in our protocol had analytical grade belonging to Merck and Sigma-Aldrich. Phosphate buffer solution (PBS) was prepared by phosphoric acid and adjusted by NaOH to the desired pH value.

### 2.3. Preparation of Hierarchical Flower-like $\text{NiCo}_2\text{O}_4$ Nanoplates

The protocol proposed by Chu et al., with slight modification, was followed to construct hierarchical flower-like  $\text{NiCo}_2\text{O}_4$  nanoplates [70]. Thus,  $\text{Ni}(\text{NO}_3)_2 \cdot 6\text{H}_2\text{O}$  (0.5 mmol, 0.145 gr),  $\text{Co}(\text{NO}_3)_2 \cdot 6\text{H}_2\text{O}$  (1 mmol, 0.291 gr),  $\text{NH}_4\text{F}$  (3 mmol, 0.111 gr), and urea (7.5 mmol, 0.45 gr) were dispersed in deionized water (40 mL) while stirring for 40 min until reaching a clear pink solution, followed by placing in a Teflon-lined stainless steel autoclave for three hours at  $120 \text{ }^\circ\text{C}$ . After cooling down to the laboratory temperature, the collected precipitate was rinsed thoroughly with deionized water and oven-dried for 12 h at  $65 \text{ }^\circ\text{C}$ . At last, the obtained product was annealed at  $350 \text{ }^\circ\text{C}$  for 150 min.

### 2.4. Preparation of the $\text{NiCo}_2\text{O}_4/\text{SPGE}$ Sensor

A drop-casting technique was followed to fabricate the  $\text{NiCo}_2\text{O}_4/\text{SPGE}$  (Scheme 1). Thus, a certain amount of as-prepared flower-like  $\text{NiCo}_2\text{O}_4$  nanoplates (1 mg) was subsequently dispersed in deionized water (1 mL) under 20-min ultra-sonication. Then, the well-dispersed suspension (5  $\mu\text{L}$ ) was coated on the SPGE surface in a dropwise manner and dried at the laboratory temperature. The electrochemical surface areas of the  $\text{NiCo}_2\text{O}_4/\text{SPGE}$  and the SPGE were obtained by CV using 1 mM  $\text{K}_3\text{Fe}(\text{CN})_6$  at various scan rates. The electro-active surface area of the modified electrode and un-modified electrode were evaluated by using the Randles–Sevcik equation. The calculated electro-chemical active surface area is  $0.15 \text{ cm}^2$ , for the  $\text{NiCo}_2\text{O}_4/\text{SPGE}$  and  $0.02 \text{ cm}^2$  for the bare SPGE.



**Scheme 1.** Schematic illustration of  $\text{NiCo}_2\text{O}_4$ /SPGE-based sunset yellow electrochemical detection.

### 2.5. Real Sample Preparation

Orange juice and apple juice were purchased from a local market. The fruit juice samples were centrifuged for 40 min at 400 rpm and then filtered. The obtained juice was diluted by PBS (pH = 7.0) and then used for real sample analysis. Moreover, the tap water specimens were filtered prior to analysis using the standard addition method.

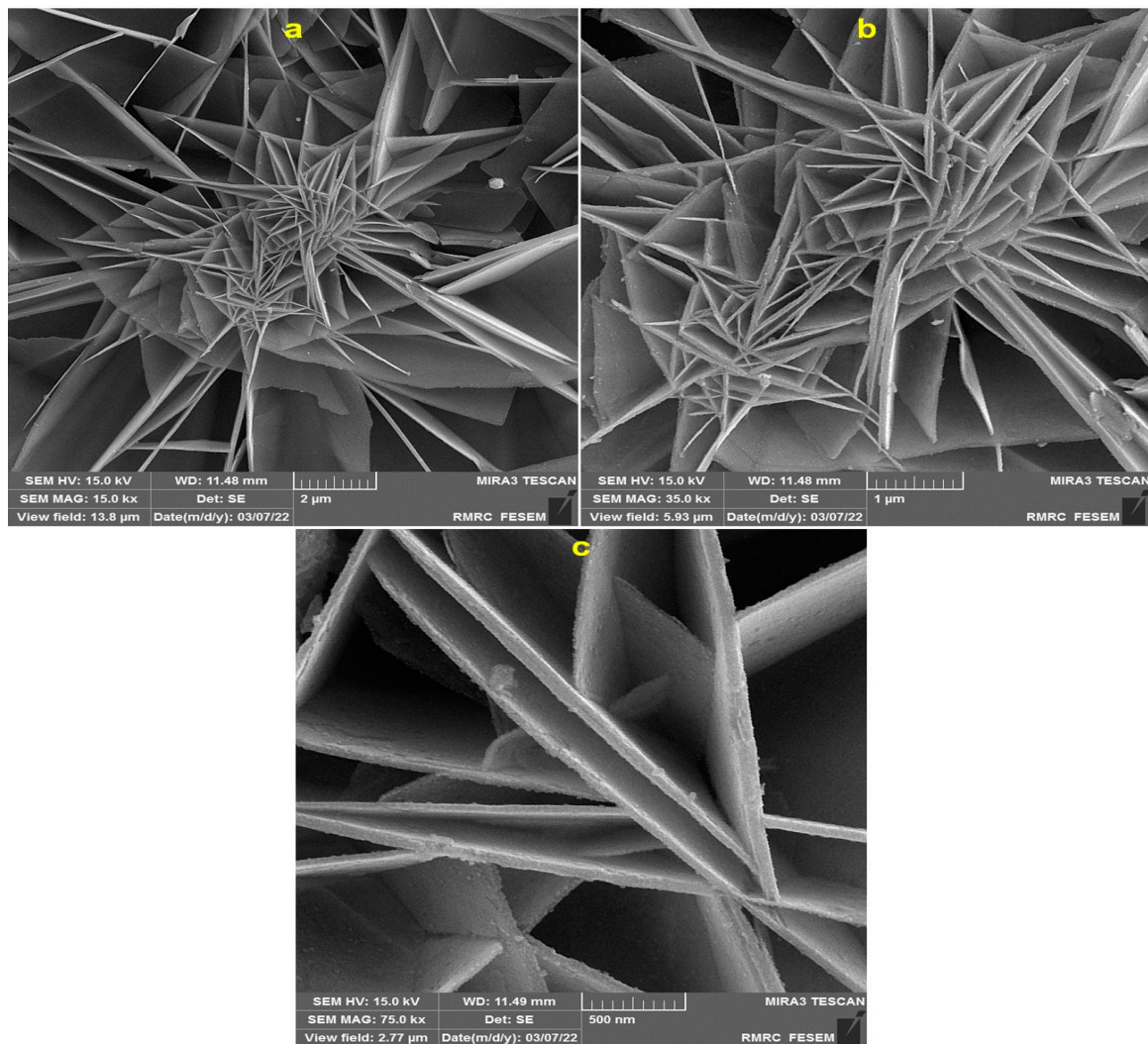
## 3. Results and Discussion

### 3.1. Characterization of Hierarchical Flower-like $\text{NiCo}_2\text{O}_4$ Nanoplates

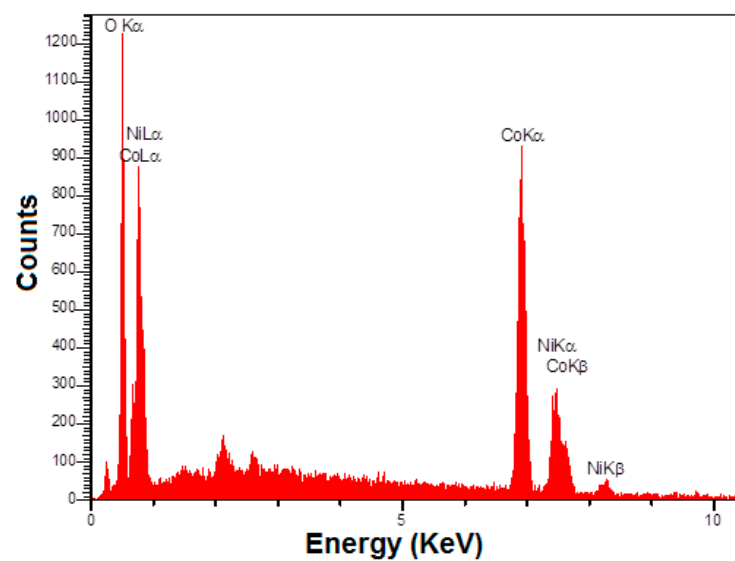
The hierarchical flower-like  $\text{NiCo}_2\text{O}_4$  nanoplates were explored for structure and morphology using FE-SEM images (Figure 1). The self-assembly of 2D  $\text{NiCo}_2\text{O}_4$  nanoplates around a center resulted in the formation of hierarchical flower-like  $\text{NiCo}_2\text{O}_4$  nanostructures. The FE-SEM image at high magnification shows the thickness of <60 nm for the produced nanoplates.

Figure 2 shows the EDS analysis in determining the chemical composition of the hierarchical flower-like  $\text{NiCo}_2\text{O}_4$  nanoplates, the findings of which display Ni, Co, and O elements present in the structure, with no impurity.

Figure 3 illustrates the XRD pattern to explore the crystal phase of hierarchical flower-like  $\text{NiCo}_2\text{O}_4$  nanoplates. The diffraction peaks at  $2\theta$  values (indexed to related plane) of  $18.9^\circ$  (111),  $31.1^\circ$  (220),  $36.6^\circ$  (311),  $38.5^\circ$  (222),  $44.5^\circ$  (400),  $55.2^\circ$  (422),  $59.0^\circ$  (511),  $64.9^\circ$  (440), and  $77.1^\circ$  (533) corresponded to the JCPDS standard pattern of  $\text{NiCo}_2\text{O}_4$  (No. 01-073-1702). The distinct crystalline nature is evident based on the intense and sharp diffraction peaks. The absence of extraneous peaks can confirm great purity of as-fabricated  $\text{NiCo}_2\text{O}_4$ .



**Figure 1.** FE-SEM images at diverse magnifications (a = 2  $\mu\text{m}$ , b = 1  $\mu\text{m}$  and c = 500 nm) for hierarchical flower-like  $\text{NiCo}_2\text{O}_4$  nanoplates.



**Figure 2.** EDS spectrum of hierarchical flower-like  $\text{NiCo}_2\text{O}_4$  nanoplates.

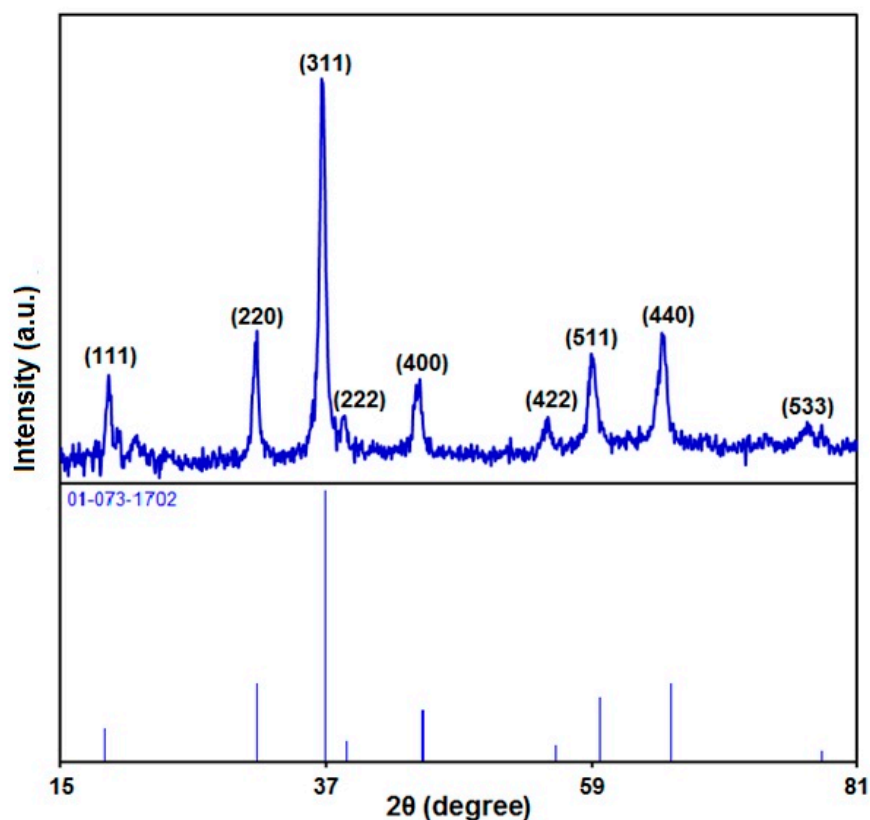


Figure 3. XRD pattern of hierarchical flower-like NiCo<sub>2</sub>O<sub>4</sub> nanoplates.

The production of NiCo<sub>2</sub>O<sub>4</sub> was further confirmed via FT-IR spectrum (Figure 4). As seen, the peaks at 3456 and 1638 cm<sup>-1</sup> were related to the characteristic hydroxyl stretching and bending vibrations in the adsorbed H<sub>2</sub>O [71]. The peaks at 557 and 641 cm<sup>-1</sup> corresponded to metal–oxygen bond vibrations in the NiCo<sub>2</sub>O<sub>4</sub> [72].

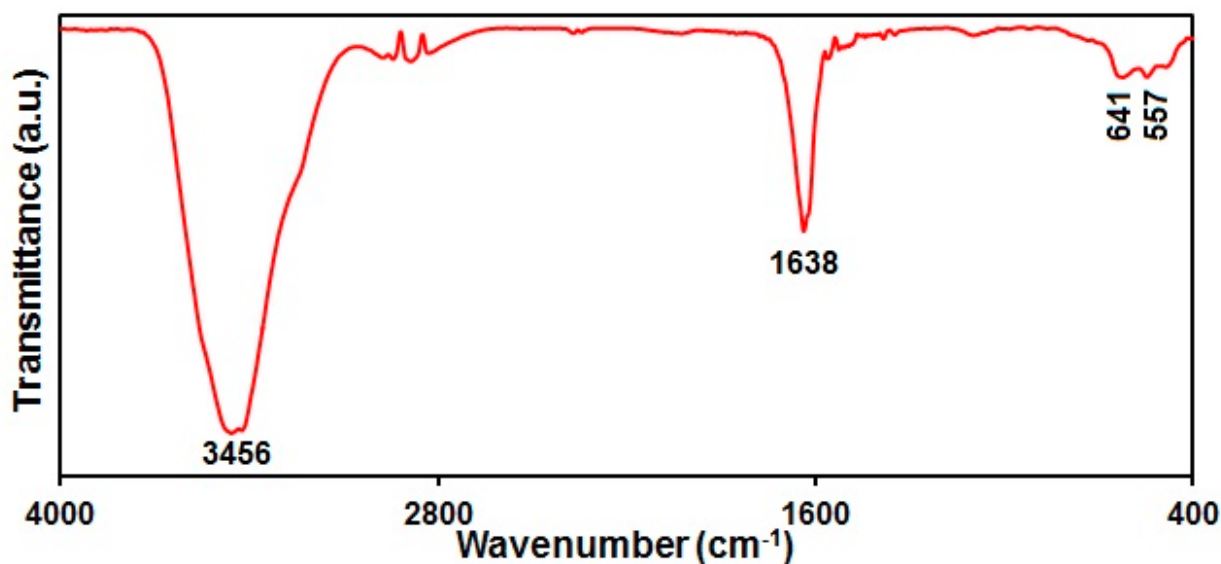
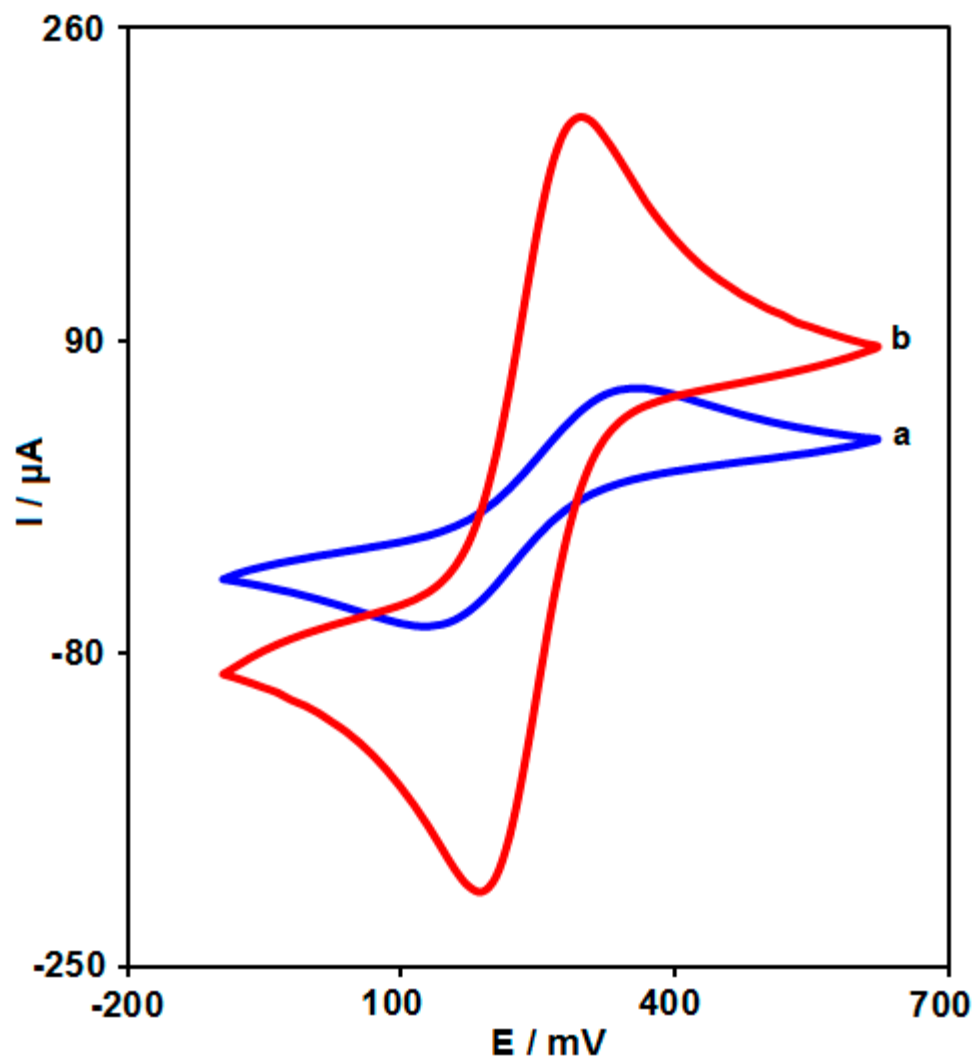


Figure 4. FT-IR spectrum of hierarchical flower-like NiCo<sub>2</sub>O<sub>4</sub> nanoplates.

### 3.2. Electrochemical Characteristics of the Modified Electrode

The electrochemical properties of the modified electrodes were studied by CV in the presence of [Fe(CN)<sub>6</sub>]<sup>3-/4-</sup> (Figure 5). Obviously, a pair of well-shaped and symmetrical redox peaks occurred at all electrodes, demonstrating that the redox behavior of Fe<sup>III</sup>/Fe<sup>II</sup>

corresponded to a quasi-reversible process. At bare SPGE, a pair of relative weak redox peaks ( $I_{pa} = 64 \mu\text{A}$ ;  $I_{pc} = -64 \mu\text{A}$ ) appeared at 0.35 and 0.115 V, respectively. After modification of SPGE by  $\text{NiCo}_2\text{O}_4$  nanoplates, the  $I_{pa}$  and  $I_{pc}$  increased to 209 and  $-209 \mu\text{A}$  while the peak separation ( $\Delta E_p$ ) decreased from 0.235 to 0.105 V.



**Figure 5.** CVs curves of different electrode in PBS (0.1 M, pH 7.0) solution containing 1.0 M KCl and 5.0 mM  $\text{Fe}(\text{CN})_6^{3-/4-}$ ; (a) bare SPGE and (b)  $\text{NiCo}_2\text{O}_4/\text{SPGE}$ . Scan rate:  $100 \text{ mV s}^{-1}$ .

### 3.3. Influence of pH on Electrochemical Behavior of Sunset Yellow

The electrochemical response of sunset yellow in the 0.1 M PBS adjusted to variable pH values (2.0 to 9.0) was explored to determine the influence of the electrolyte solution pH (Figure 6). The results showed that the peak current of sunset yellow oxidation depended on the pH value, so that it reached a maximum with increasing pH up to 7.0 and then decreased with further pH values. Hence, the pH value of 7.0 was considered to be the optimum for subsequent electrochemical determinations (Figure 6, inset). Since the equal amount of proton and electron participates in the redox process, the electrochemical reaction of sunset yellow is 1 electron and 1 proton process. Hence, the electrochemical mechanism of sunset yellow on the  $\text{NiCo}_2\text{O}_4/\text{SPGE}$  can be inferred from Scheme 2.

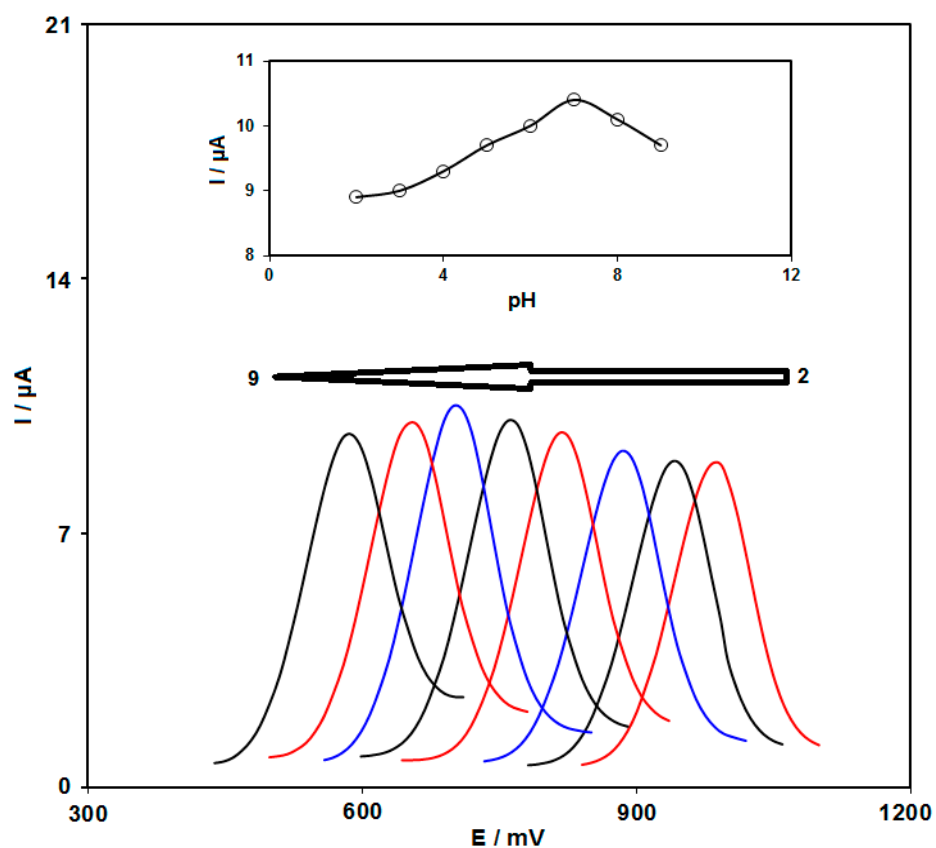
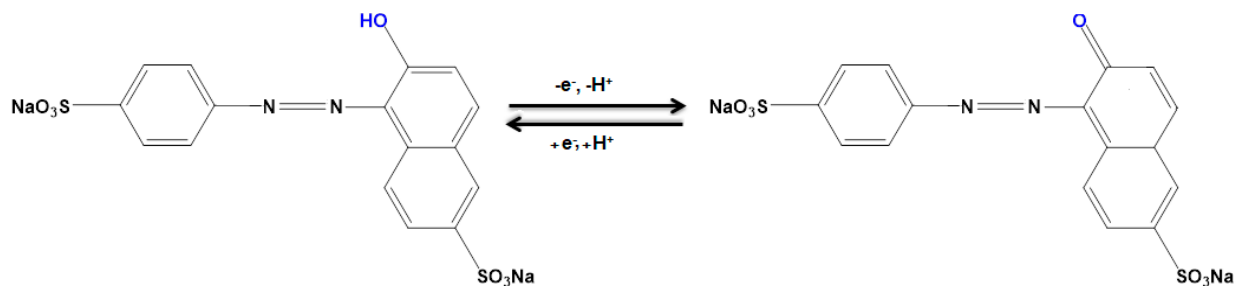


**Figure 6.** DPVs captured for the oxidation of 100.0  $\mu\text{M}$  sunset yellow contents on the  $\text{NiCo}_2\text{O}_4/\text{SPGE}$  at variable pH (2.0, 3.0, 4.0, 5.0, 6.0, 7.0, 8.0 and 9.0). Inset: Variation peak current as a function of solution pH.



**Scheme 2.** The mechanism of the electrochemical reaction of sunset yellow on the  $\text{NiCo}_2\text{O}_4/\text{SPGE}$ .

### 3.4. Electrochemical Response of Sunset Yellow at Various Electrodes

The CVs were captured for the sunset yellow (100.0  $\mu\text{M}$ ) electrochemical reaction on the bare SPGE and  $\text{NiCo}_2\text{O}_4$ -modified SPGE to explore the electrocatalytic performance of the hierarchical flower-like  $\text{NiCo}_2\text{O}_4$  nanoplates (Figure 7). Figure 7 illustrates the weak oxidation peak on the bare SPGE ( $I_{pa} = 3.1 \mu\text{A}$ ), whereas  $\text{NiCo}_2\text{O}_4$ -modified SPGE had a significant improvement in the current ( $I_{pa} = 10.5 \mu\text{A}$ ). This significant improvement in the oxidation peak can appear because of the appreciable catalytic impact of hierarchical flower-like  $\text{NiCo}_2\text{O}_4$  nanoplates for the sunset yellow electrochemical reaction.

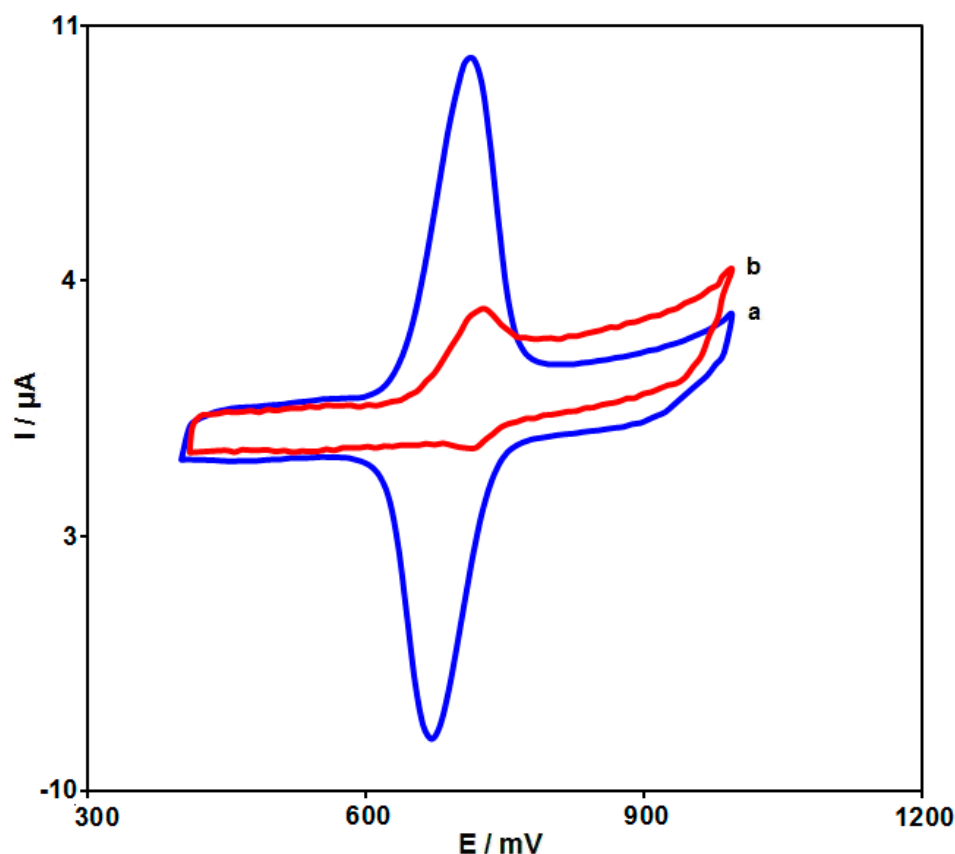


**Figure 7.** CVs captured for electrochemical reaction of sunset yellow (100.0  $\mu\text{M}$ ) in PBS (0.1 M; pH = 7.0) on (a)  $\text{NiCo}_2\text{O}_4/\text{SPGE}$  and (b) unmodified SPGE with the scan rate of 50 mV/s.

### 3.5. Effect of Scan Rate

The LSVs were captured for the oxidation of sunset yellow (60.0  $\mu\text{M}$ ) on the  $\text{NiCo}_2\text{O}_4/\text{SPGE}$  under variable scan rates (Figure 8). There was an apparent gradual elevation in the oxidation peak when the scan rate ranged from 10 to 300 mV/s. As seen in Figure 8 (Inset), the anodic peak current ( $I_{pa}$ ) had a linear association with the square root of the scan rate ( $v^{1/2}$ ). The regression equation was obtained to be  $I_{pa} (\mu\text{A}) = 1.0663 v^{1/2} (\text{mV s}^{-1})^{1/2} - 1.3594$  ( $R^2 = 0.9995$ ), meaning a controlled diffusion process of the sunset yellow oxidation on the  $\text{NiCo}_2\text{O}_4/\text{SPGE}$  (Figure 8, Inset A). In addition, the variation of the logarithm of the current as a function of the variation in the logarithm of the scan rate showed a linear behavior that showed the controlled diffusion process of the sunset yellow oxidation on the  $\text{NiCo}_2\text{O}_4/\text{SPGE}$  (Figure 8, Inset B).

A Tafel plot (Figure 9 (Inset)) was achieved on the basis of data related to the rising domain of the current–voltage curve at a low scan rate (10 mV/s) for sunset yellow (60.0  $\mu\text{M}$ ) to explore the rate-determining step. The linearity of E vs.  $\log I$  plot clarifies the involvement of electrode process kinetics. The slope from this plot could present the count of transferred electrons during the rate-determining step. Based on Figure 9 (inset), the Tafel slope was estimated to be 0.1309 V for the linear domain of the plot. The slope of the Tafel plot was equal to  $2.3RT/n(1-\alpha)F$ , and the Tafel slope based on Figure 9 (inset) was estimated to be 0.1309 V for the linear domain of the plot. The Tafel slope value reveals that the rate-limiting step is the one-electron transfer process, considering a transfer coefficient ( $\alpha$ ) of 0.55.

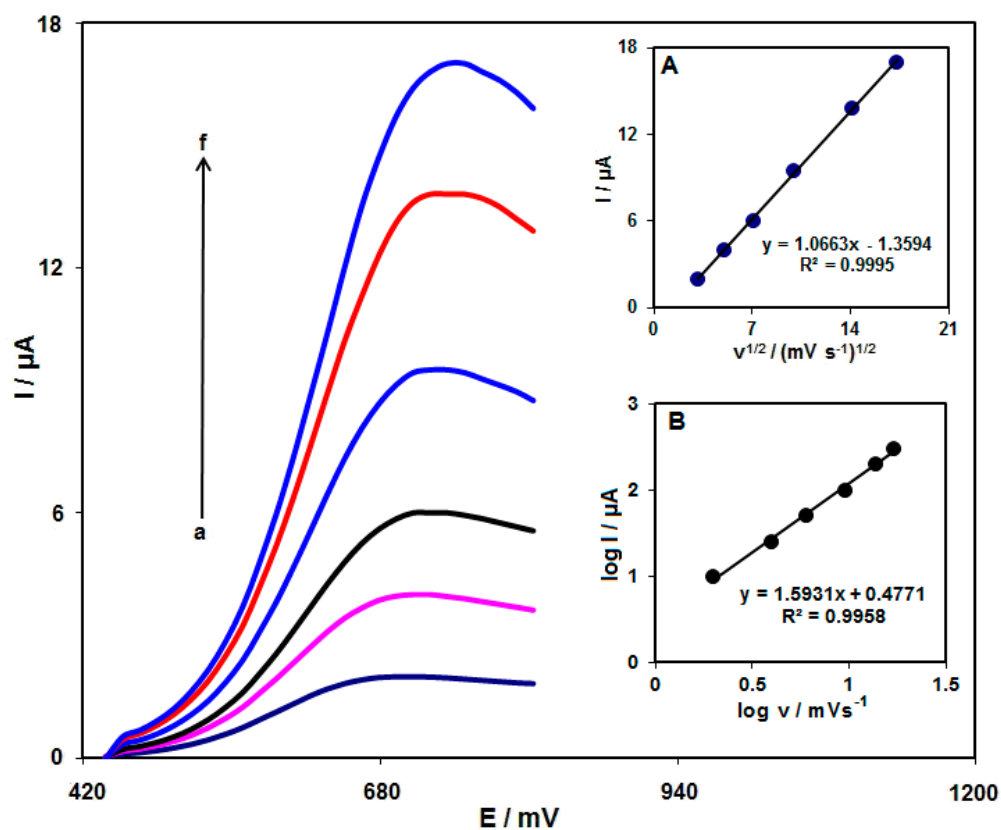


**Figure 8.** LSVs captured for the oxidation of sunset yellow (60.0 μM) on the NiCo<sub>2</sub>O<sub>4</sub>/SPGE under variable scan rates (a: 10 mV/s, b: 25 mV/s, c: 50 mV/s, d: 100 mV/s, e: 200 mV/s, and f: 300 mV/s). Insets: (A) the correlation of I<sub>pa</sub> with v<sup>1/2</sup>. (B) Variation of logarithm of current as a function of variation in the logarithm of scan rate.

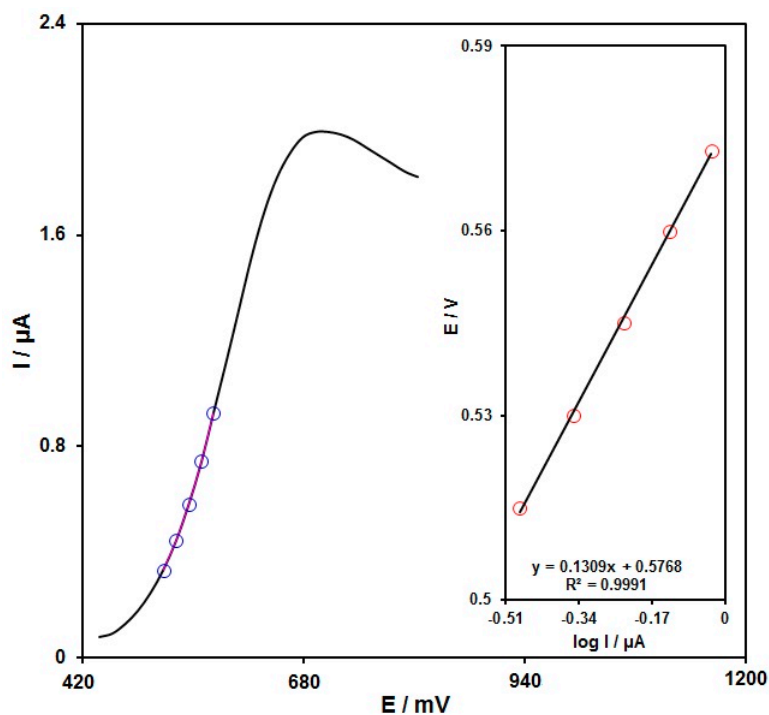


**Figure 9.** LSV for sunset yellow (60.0 μM) at the scan rate of 10 mV/s. Inset: The Tafel plot from the rising domain of the respective voltammogram.

### 3.6. Chronoamperometric Analysis

Chronoamperometry was used to explore the sunset yellow catalytic oxidation on the NiCo<sub>2</sub>O<sub>4</sub>/SPGE surface. Chronoamperometric analysis was done for variable sunset yellow contents on NiCo<sub>2</sub>O<sub>4</sub>/SPGE at the working electrode potential of 740 mV. The chronoamperograms captured for variable sunset yellow contents on the NiCo<sub>2</sub>O<sub>4</sub>/SPGE can be seen in Figure 10. Cottrell's equation explains the current (I) for electrochemical reaction of an electroactive material with a D value (diffusion coefficient) under a mass transport-limited condition. Figure 10A shows a linear relationship of the I value with  $t^{-1/2}$  for the oxidation of variable sunset yellow contents. The slopes from the obtained straight lines were plotted against variable sunset yellow contents (Figure 10B). The plotted slope and Cottrell equation ( $I = nFAD^{1/2}C_b\pi^{-1/2}t^{-1/2}$ ) estimated the D value to be  $9.2 \times 10^{-5} \text{ cm}^2/\text{s}$  for sunset yellow. The mean D value in this work is comparable with the results published in other papers [73,74].

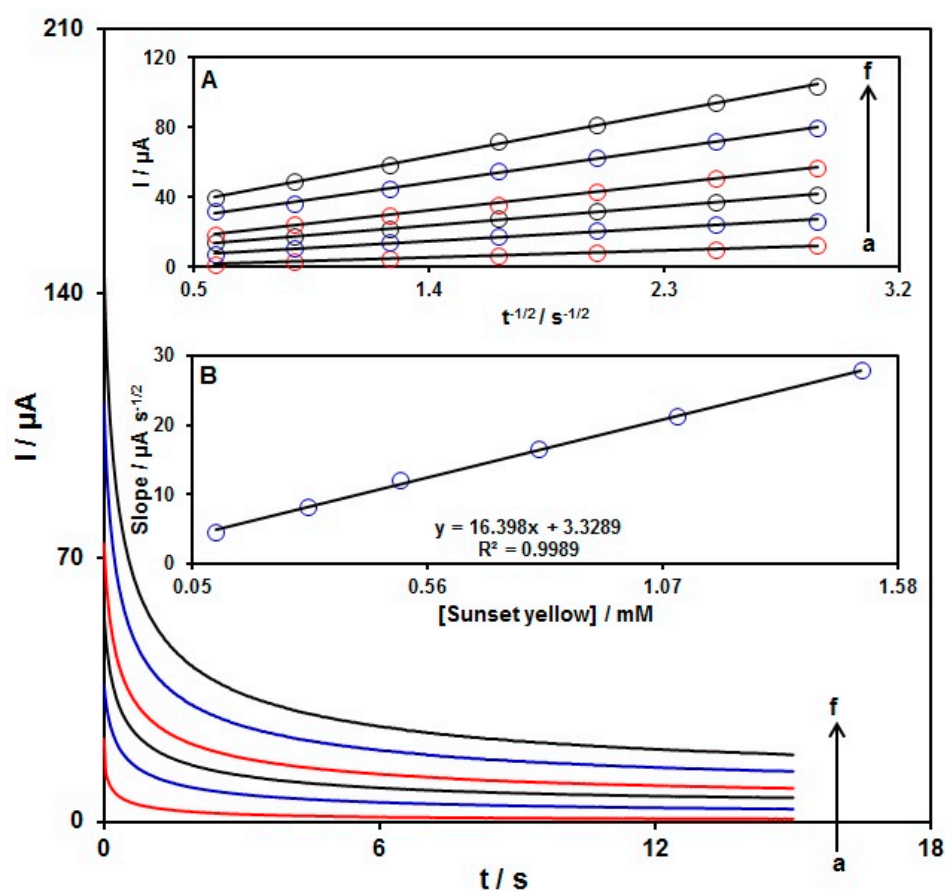


**Figure 10.** Chronoamperometric behavior of NiCo<sub>2</sub>O<sub>4</sub>/SPGE in PBS (0.1 M; pH = 7.0) at potential of 740 mV for variable sunset yellow contents (a: 0.1 mM, b: 0.3 mM, c: 0.5 mM, d: 0.8 mM, e: 1.1 mM and f: 1.5 mM). Insets: (A) Plots of  $I$  vs.  $t^{-1/2}$  and (B) plots of the slopes from the straight lines vs. sunset yellow level.

### 3.7. DPV Analysis of Sunset Yellow

DPV analysis was done for variable sunset yellow contents to explore the linear dynamic range, LOD, and sensitivity of the NiCo<sub>2</sub>O<sub>4</sub>/SPGE under optimized experimental circumstances (Figure 11). As expected, the elevation in the sunset yellow level enhanced the peak current. Figure 11 (Inset) shows a linear behavior of the oxidation peak currents and variable sunset yellow contents (0.02  $\mu\text{M}$  to 145.0  $\mu\text{M}$ ) with the linear regression equation of  $I_{pa} (\mu\text{A}) = 0.1009C_{\text{sunset yellow}} + 0.4534$  ( $R^2 = 0.9999$ ), and the sensitivity of 0.67  $\mu\text{A}/(\mu\text{M}\cdot\text{cm}^2)$ . In the equations of  $\text{LOD} = 3S_b/m$  and  $\text{LOQ} = 10S_b/m$ , the  $S_b$  stands for the standard deviation of the response for blank solution, and  $m$  for the slope from

the standard graph. The LOD and LOQ were estimated at 0.008 and 0.024  $\mu\text{M}$  for sunset yellow determination on  $\text{NiCo}_2\text{O}_4/\text{SPGE}$ .

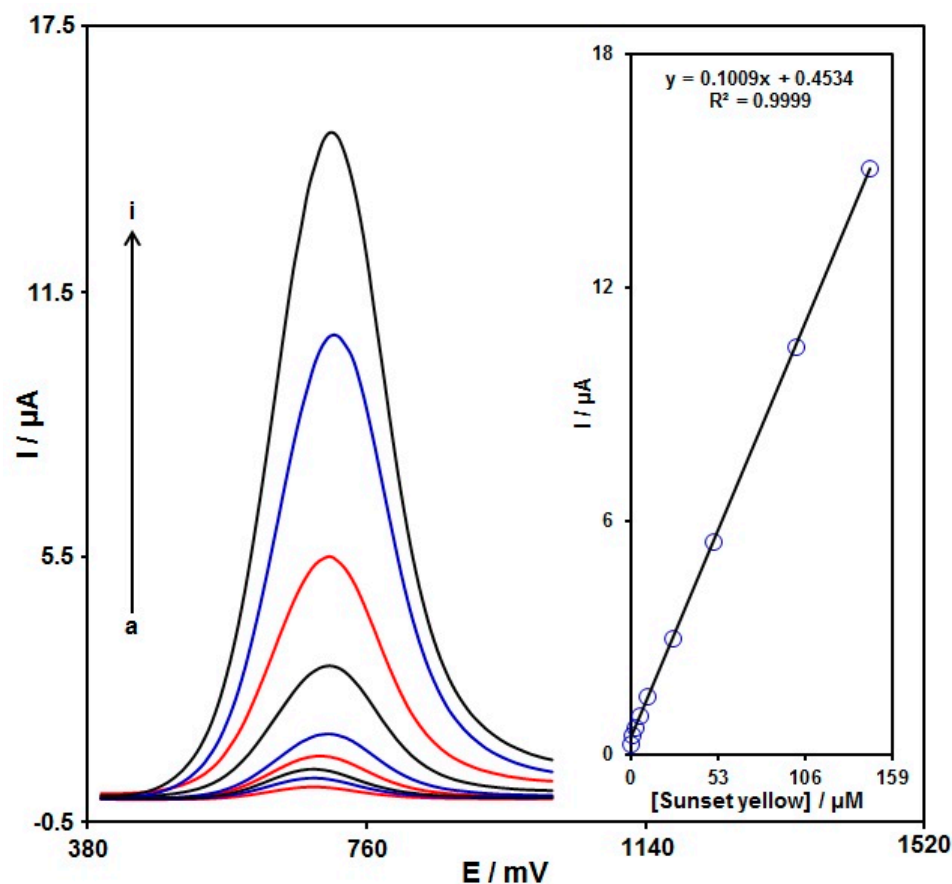


**Figure 11.** DPVs captured for the oxidation of variable sunset yellow contents on the  $\text{NiCo}_2\text{O}_4/\text{SPGE}$  (a: 0.02  $\mu\text{M}$ , b: 0.2  $\mu\text{M}$ , c: 2.0  $\mu\text{M}$ , d: 5.0  $\mu\text{M}$ , e: 10.0  $\mu\text{M}$ , f: 25.0  $\mu\text{M}$ , g: 50.0  $\mu\text{M}$ , h: 100.0  $\mu\text{M}$ , and i: 145.0  $\mu\text{M}$ ). Inset: Calibration curve of voltammetric response (Ipa) against sunset yellow level.

Table 1 compares the efficiency of the sunset yellow sensor prepared by the hierarchical flower-like  $\text{NiCo}_2\text{O}_4$  nanoplates-modified SPGE and other reported works [1,75–79].

**Table 1.** Comparison of the efficiency of the  $\text{NiCo}_2\text{O}_4/\text{SPGE}$  with other reported modified electrodes for sunset yellow determination.

| Electrochemical Sensor   | Method | Linear Range/ $\mu\text{M}$ | LOD/ $\mu\text{M}$ | Ref.      |
|--|--------|-----------------------------|--------------------|-----------|
| Chitosan (CHIT)-graphene (Gr)/glassy carbon electrode (GCE)  | CV     | 0.2–100.0                   | 0.066              | [1]       |
| Multi-walled carbon nanotubes (MWCNTs)/GCE   | DPV    | 0.55–7.0                    | 0.12               | [75]      |
| Au nanoparticles (NPs)/carbon paste electrode (CPE)  | DPV    | 0.1–2.0                     | 0.03               | [76]      |
| Reduced graphene oxide (rGO)-Ni-BTC metal-organic framework (MOF)/Screen-printed carbon electrode (SPCE) | DPV    | 0.05–5.0                    | 0.025              | [77]      |
| Ionic liquid (IL)- $\text{NiFe}_2\text{O}_4$ -rGO/CPE  | DPV    | 0.05–30.0 and 30.0–500.0    | 0.03               | [78]      |
| Electrochemically reduced oxide (ErGO)/GCE   | DPV    | 0.05–1.0                    | 0.0192             | [79]      |
| $\text{NiCo}_2\text{O}_4/\text{SPGE}$  | DPV    | 0.02–145.0                  | 0.008              | This Work |

### 3.8. Repeatability, Reproducibility, and Stability

The  $\text{NiCo}_2\text{O}_4/\text{SPGE}$  was examined for repeatability through the measurement of the response of 50.0  $\mu\text{M}$  sunset yellow on the surface of the same electrode for 10 times.

The relative standard deviation (RSD) of 3.4% for the current response of sunset yellow demonstrates the good repeatability of the proposed electrode.

To test the reproducibility, five NiCo<sub>2</sub>O<sub>4</sub>/SPGEs produced by the same procedures were applied to measure 50.0 μM sunset yellow under identical circumstances; the obtained RSD of 5.9% meant commendable reproducibility (Figure 12).

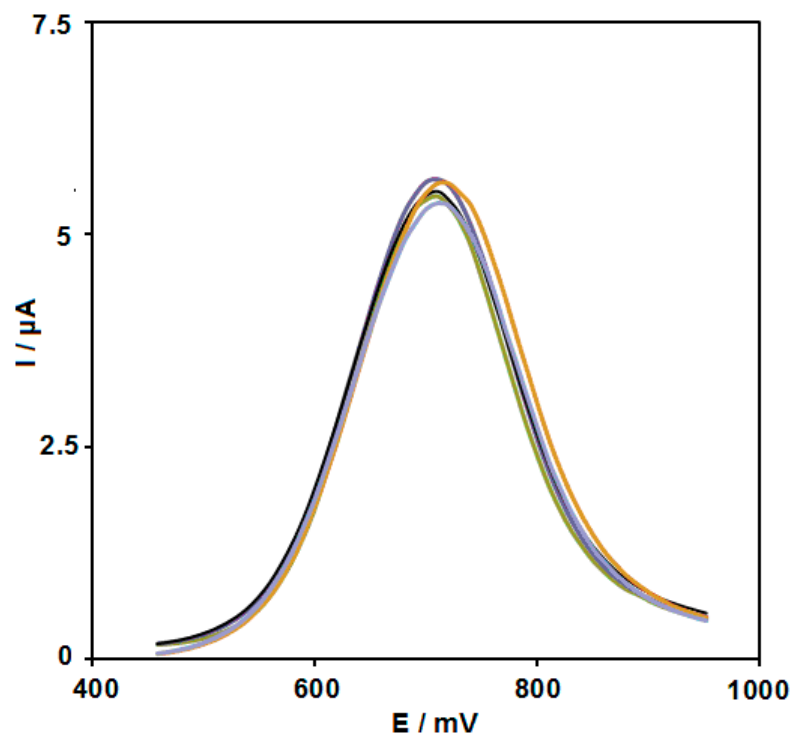


**Figure 12.** DPVs captured for the oxidation of 50.0 μM sunset yellow contents on the five constructed NiCo<sub>2</sub>O<sub>4</sub>/SPGEs.

To test the NiCo<sub>2</sub>O<sub>4</sub>/SPGE stability, the current responses of 50.0 μM sunset yellow were measured following 14-day storage of the sensor at ambient temperature. The decrease in the peak current of sunset yellow to 95.8% of its original response demonstrated appreciable stability.

### 3.9. Interference Studies

The anti-interference of the NiCo<sub>2</sub>O<sub>4</sub>/SPGE was evaluated by measuring the DPV responses of 50.0 μM sunset yellow with diverse interference matrices. The tolerance limit was defined as the maximum concentration of the interfering substance that caused an approximately ±5% relative error in the determination. It was found that 200-fold Ca<sup>2+</sup>, NH<sub>4</sub><sup>+</sup>, Mn<sup>2+</sup>, Al<sup>3+</sup>, Fe<sup>3+</sup>, Zn<sup>2+</sup>, Br<sup>-</sup>, Mg<sup>2+</sup>, SO<sub>4</sub><sup>2-</sup>, and CO<sub>3</sub><sup>2-</sup> and 20-fold starch, sucrose, uric acid, glucose, vitamin B<sub>6</sub>, vitamin B<sub>2</sub>, dopamine, citric acid, and ascorbic acid had no effect on the determination of the sunset yellow. Hence, the proposed sensor has a good selectivity for sunset yellow.

### 3.10. Analysis of Real Specimens

The practical applicability of NiCo<sub>2</sub>O<sub>4</sub>/SPGE was tested by sensing sunset yellow in orange juice, apple juice, and tap water specimens using the DPV procedure and the standard addition method. The results can be seen in Table 2. The recovery rate was between 96.4% and 104.0%, and all RSD values were ≤3.5%. According to the experimental results, the NiCo<sub>2</sub>O<sub>4</sub>/SPGE sensor possessed a high potential for practical applicability.

**Table 2.** Voltammetric sensing of sunset yellow in real specimens using NiCo<sub>2</sub>O<sub>4</sub>/SPGE. All concentrations are in  $\mu\text{M}$  ( $n = 5$ ).

| Sample       | Spiked | Found | Recovery (%) | R.S.D. (%) |
|--------------|--------|-------|--------------|------------|
| Apple Juice  | 0      | 2.5   | -            | 3.2        |
|              | 2.0    | 4.6   | 102.2        | 2.7        |
|              | 3.0    | 5.3   | 96.4         | 1.9        |
|              | 4.0    | 6.4   | 98.5         | 2.9        |
|              | 5.0    | 7.6   | 101.3        | 3.0        |
| Orange juice | 0      | 3.8   | -            | 2.7        |
|              | 1.0    | 4.7   | 97.9         | 3.5        |
|              | 2.0    | 6.0   | 103.4        | 3.1        |
|              | 3.0    | 6.9   | 101.5        | 1.7        |
|              | 4.0    | 7.7   | 98.7         | 2.5        |
| Tap Water    | 0      | -     | -            | -          |
|              | 5.0    | 5.1   | 102.0        | 2.8        |
|              | 7.5    | 7.4   | 98.7         | 3.4        |
|              | 10.0   | 10.4  | 104.0        | 1.8        |
|              | 12.5   | 12.4  | 99.2         | 2.6        |

#### 4. Conclusions

The current attempt was made to construct an effective electrochemical sensing system for detection of sunset yellow via the modification of SPGE with hierarchical flower-like NiCo<sub>2</sub>O<sub>4</sub> nanoplates (NiCo<sub>2</sub>O<sub>4</sub>/SPGE sensor). The proposed sensor was constructed by a facile and effective drop-casting protocol. Large surface area, high catalytic activity, and great conductivity of flower-like NiCo<sub>2</sub>O<sub>4</sub> nanoplates provided a good catalytic activity for the NiCo<sub>2</sub>O<sub>4</sub>/SPGE towards the sunset yellow with increased peak current of oxidation and reduced overpotential of oxidation. Electrochemical determinations presented appreciable performance for the modified electrode in the sunset yellow detection at the pH value of 7.0. The as-fabricated NiCo<sub>2</sub>O<sub>4</sub>/SPGE had outstanding analytical response for the sunset yellow detection in a broad linearity range from 0.02  $\mu\text{M}$  to 145.0  $\mu\text{M}$  with a commendable sensitivity of 0.67  $\mu\text{A}/(\mu\text{M}\cdot\text{cm}^2)$  and the LOD as low as 0.008  $\mu\text{M}$ . The practical applicability of the proposed sensor was verified by determining sunset yellow in real matrices, with satisfactory results. The proposed method could be applied to food quality control, and presents a rapid, inexpensive, and environmental-friendly alternative to separation methods.

**Author Contributions:** Conceptualization, H.B.; methodology, S.T. and Z.D.; formal analysis, S.T. and F.G.N.; investigation, H.B.; writing—original draft preparation, H.B., S.T., Z.D. and F.G.N.; writing—review and editing, H.B., S.T., Z.D. and F.G.N.; supervision, H.B.; project administration, H.B.; funding acquisition, H.B. All authors have read and agreed to the published version of the manuscript.

**Funding:** Authors acknowledge the financial support provided for this project (No. 7.S.01.1020) by the Institute of Science and High Technology and Environmental Sciences, Graduate University of Advanced Technology, Kerman, Iran.

**Institutional Review Board Statement:** Not applicable.

**Informed Consent Statement:** Not applicable.

**Data Availability Statement:** The data presented in this study are available on request from the corresponding authors.

**Acknowledgments:** The authors acknowledge the financial support provided for this project (No. 7.S.01.1020) by the Institute of Science and High Technology and Environmental Sciences, Graduate University of Advanced Technology, Kerman, Iran.

**Conflicts of Interest:** The authors declare no conflict of interest.

## References

1. Magerusan, L.; Pogacean, F.; Coros, M.; Socaci, C.; Pruneanu, S.; Leostean, C.; Pana, I.O. Green methodology for the preparation of chitosan/graphene nanomaterial through electrochemical exfoliation and its applicability in Sunset Yellow detection. *Electrochim. Acta* **2018**, *283*, 578–589. [[CrossRef](#)]
2. Karimi-Maleh, H.; Beitollahi, H.; Kumar, P.S.; Tajik, S.; Mohammadzadeh-Jahani, P.; Karimi, F.; Zare, N. Recent advances in carbon nanomaterials-based electrochemical sensors for food azo dyes detection. *Food Chem. Toxicol.* **2022**, *164*, 112961. [[CrossRef](#)] [[PubMed](#)]
3. Wang, J.; Yang, B.; Wang, H.; Yang, P.; Du, Y. Highly sensitive electrochemical determination of Sunset Yellow based on gold nanoparticles/graphene electrode. *Anal. Chim. Acta* **2015**, *893*, 41–48. [[CrossRef](#)] [[PubMed](#)]
4. Tahtaisleyen, S.; Gorduk, O.; Sahin, Y. Electrochemical determination of sunset yellow using an electrochemically prepared graphene oxide modified–pencil graphite electrode (EGO-PGE). *Anal. Lett.* **2021**, *54*, 394–416. [[CrossRef](#)]
5. Karimi-Maleh, H.; Darabi, R.; Shabani-Nooshabadi, M.; Baghayeri, M.; Karimi, F.; Rouhi, J.; Karaman, C. Determination of D&C Red 33 and Patent Blue V Azo dyes using an impressive electrochemical sensor based on carbon paste electrode modified with ZIF-8/g-C<sub>3</sub>N<sub>4</sub>/Co and ionic liquid in mouthwash and toothpaste as real samples. *Food Chem. Toxicol.* **2022**, *162*, 112907.
6. Zhang, K.; Luo, P.; Wu, J.; Wang, W.; Ye, B. Highly sensitive determination of Sunset Yellow in drink using a poly (l-cysteine) modified glassy carbon electrode. *Anal. Methods* **2013**, *5*, 5044–5050. [[CrossRef](#)]
7. Nguyen, Q.T.; Le, T.G.; Bergonzo, P.; Tran, Q.T. One-step fabrication of nickel-electrochemically reduced graphene oxide nanocomposites modified electrodes and application to the detection of sunset yellow in drinks. *Appl. Sci.* **2022**, *12*, 2614. [[CrossRef](#)]
8. Ding, Z.; Deng, P.; Wu, Y.; Tian, Y.; Li, G.; Liu, J.; He, Q. A novel modified electrode for detection of the food colorant sunset yellow based on nanohybrid of MnO<sub>2</sub> nanorods-decorated electrochemically reduced graphene oxide. *Molecules* **2019**, *24*, 1178. [[CrossRef](#)]
9. Al-Degs, Y.S. Determination of three dyes in commercial soft drinks using HPLC/GO and liquid chromatography. *Food Chem.* **2009**, *117*, 485–490. [[CrossRef](#)]
10. He, Q.; Liu, J.; Liu, X.; Xia, Y.; Li, G.; Deng, P.; Chen, D. Novel electrochemical sensors based on cuprous oxide-electrochemically reduced graphene oxide nanocomposites modified electrode toward sensitive detection of sunset yellow. *Molecules* **2018**, *23*, 2130. [[CrossRef](#)]
11. Wang, Z.; Shan, Y.; Xu, L.; Wu, G.; Lu, X. Development and application of the tartrazine voltammetric sensors based on molecularly imprinted polymers. *Int. J. Polym. Anal. Charact.* **2017**, *22*, 83–91. [[CrossRef](#)]
12. Sha, O.; Zhu, X.; Feng, Y.; Ma, W. Determination of sunset yellow and tartrazine in food samples by combining ionic liquid-based aqueous two-phase system with high performance liquid chromatography. *J. Anal. Methods Chem.* **2014**, *2014*, 964273. [[CrossRef](#)] [[PubMed](#)]
13. Lancaster, F.E.; Lawrence, J.F. Determination of benzidine in the food colours tartrazine and sunset yellow FCF, by reduction and derivatization followed by high-performance liquid chromatography. *Food Addit. Contam.* **1999**, *16*, 381–390. [[CrossRef](#)]
14. El-Shahawi, M.S.; Hamza, A.; Al-Sibaai, A.A.; Bashammakh, A.S.; Al-Saidi, H.M. A new method for analysis of sunset yellow in food samples based on cloud point extraction prior to spectrophotometric determination. *J. Ind. Eng. Chem.* **2013**, *19*, 529–535. [[CrossRef](#)]
15. Ma, K.; Li, X.J.; Wang, H.F.; Zhao, M. Rapid and sensitive method for the determination of eight food additives in red wine by ultra-performance liquid chromatography tandem mass spectrometry. *Food Anal. Methods* **2015**, *8*, 203–212. [[CrossRef](#)]
16. Fuh, M.R.; Chia, K.J. Determination of sulfonated azo dyes in food by ion-pair liquid chromatography with photodiode array and electrospray mass spectrometry detection. *Talanta* **2002**, *56*, 663–671. [[CrossRef](#)]
17. Huang, H.Y.; Shih, Y.C.; Chen, Y.C. Determining eight colorants in milk beverages by capillary electrophoresis. *J. Chromatogr. A* **2002**, *959*, 317–325. [[CrossRef](#)]
18. Soponar, F.; Moç, A.C.; Sârbu, C. Quantitative determination of some food dyes using digital processing of images obtained by thin-layer chromatography. *J. Chromatogr. A* **2008**, *1188*, 295–300. [[CrossRef](#)]
19. Kaya, S.I.; Cetinkaya, A.; Ozkan, S.A. Latest advances on the nanomaterials-based electrochemical analysis of azo toxic dyes Sunset Yellow and Tartrazine in food samples. *Food Chem. Toxicol.* **2021**, *156*, 112524. [[CrossRef](#)]
20. Kouadio, K.E.; Kambiré, O.; Koffi, K.S.; Ouattara, L. Electrochemical oxidation of paracetamol on boron-doped diamond electrode: Analytical performance and paracetamol degradation. *J. Electrochem. Sci. Eng.* **2021**, *11*, 71–86.
21. Motahharinia, M.; Zamani, H.A.; Karimi Maleh, H. A sensitive electroanalytical sensor amplified with Pd-ZnO nanoparticle for determination of Sunset Yellow in real samples. *Eurasian Chem. Commun.* **2020**, *2*, 760–770. [[CrossRef](#)]
22. Rajabi, N.; Masrounia, M.; Abedi, M. Potentiometric determination of La(III) using chitosan modified carbon paste electrode with an experimental design. *Chem. Methodol.* **2020**, *4*, 660–670.
23. Shamsi, A.; Ahour, F. Electrochemical sensing of thioridazine in human serum samples using modified glassy carbon electrode. *Adv. J. Chem. A* **2020**, *4*, 22–31.
24. Karimi-Maleh, H.; Karimi, F.; Orooji, Y.; Mansouri, G.; Razmjou, A.; Aygun, A.; Sen, F. A new nickel-based co-crystal complex electrocatalyst amplified by NiO doped Pt nanostructure hybrid; a highly sensitive approach for determination of cysteamine in the presence of serotonin. *Sci. Rep.* **2020**, *10*, 11699. [[CrossRef](#)] [[PubMed](#)]

25. Arfin, T.; Rangari, S.N. Graphene oxide–ZnO nanocomposite modified electrode for the detection of phenol. *Anal. Methods* **2018**, *10*, 347–358. [[CrossRef](#)]
26. Kumar, H.; Kumari, N.; Sharma, R. Nanocomposites (conducting polymer and nanoparticles) based electrochemical biosensor for the detection of environment pollutant: Its issues and challenges. *Environ. Impact Assess. Rev.* **2020**, *85*, 106438. [[CrossRef](#)]
27. Petrović, S.; Guzsavány, V.; Ranković, N.; Beljin, J.; Rončević, S.; Dalmacija, B.; Vytřas, K. Trace level voltammetric determination of Zn (II) in selected nutrition related samples by bismuth-oxochloride-multiwalled carbon nanotube composite based electrode. *Microchem. J.* **2019**, *146*, 178–186. [[CrossRef](#)]
28. Mohanraj, J.; Durgalakshmi, D.; Rakkesh, R.A.; Balakumar, S.; Rajendran, S.; Karimi-Maleh, H. Facile synthesis of paper based graphene electrodes for point of care devices: A double stranded DNA (dsDNA) biosensor. *J. Colloid Interface Sci.* **2020**, *566*, 463–472. [[CrossRef](#)] [[PubMed](#)]
29. Payehghadr, M.; Taherkhani, Y.; Maleki, A.; Nourifard, F. Selective and sensitive voltammetric sensor for methocarbamol determination by molecularly imprinted polymer modified carbon paste electrode. *Eurasian Chem. Commun.* **2020**, *2*, 982–990.
30. Ramachandran, R.; Chen, T.W.; Chen, S.M.; Baskar, T.; Kannan, R.; Elumalai, P.; Dinakaran, K. A review of the advanced developments of electrochemical sensors for the detection of toxic and bioactive molecules. *Inorg. Chem. Front.* **2019**, *6*, 3418–3439. [[CrossRef](#)]
31. Miraki, M.; Karimi-Maleh, H.; Taher, M.A.; Cheraghi, S.; Karimi, F.; Agarwal, S.; Gupta, V.K. Voltammetric amplified platform based on ionic liquid/NiO nanocomposite for determination of benserazide and levodopa. *J. Mol. Liq.* **2019**, *278*, 672–676. [[CrossRef](#)]
32. Tajik, S.; Beitollahi, H.; Torkzadeh-Mahani, M. Electrochemical immunosensor for the detection of anti-thyroid peroxidase antibody by gold nanoparticles and ionic liquid-modified carbon paste electrode. *J. Nanostruct. Chem.* **2022**, *12*, 581–588. [[CrossRef](#)]
33. Winiarski, J.P.; Tavares, B.F.; de Fátima Ulbrich, K.; de Campos, C.E.M.; Souza, A.A.; Souza, S.M.G.U.; Jost, C.L. Development of a multianalyte electrochemical sensor for depression biomarkers based on a waste of the steel industry for a sustainable and one-step electrode modification. *Microchem. J.* **2022**, *175*, 107141. [[CrossRef](#)]
34. Fanjul-Bolado, P.; Queipo, P.; Lamas-Ardisana, P.J.; Costa-García, A. Manufacture and evaluation of carbon nanotube modified screen-printed electrodes as electrochemical tools. *Talanta* **2007**, *74*, 427–433. [[CrossRef](#)]
35. Economou, A. Screen-printed electrodes modified with “green” metals for electrochemical stripping analysis of toxic elements. *Sensors* **2018**, *18*, 1032. [[CrossRef](#)] [[PubMed](#)]
36. Mohammadzadeh Jahani, P.; Garkani Nejad, F.; Dourandish, Z.; Poursoltani Zarandi, M.; Safizadeh, M.M.; Tajik, S.; Beitollahi, H. A modified carbon paste electrode with N-rGO/CuO nanocomposite and ionic liquid for the efficient and cheap voltammetric sensing of hydroquinone in water specimens. *Chemosphere* **2022**, *302*, 134712. [[CrossRef](#)] [[PubMed](#)]
37. Rowley-Neale, S.J.; Brownson, D.A.; Smith, G.; Banks, C.E. Graphene oxide bulk-modified screen-printed electrodes provide beneficial electroanalytical sensing capabilities. *Biosensors* **2020**, *10*, 27. [[CrossRef](#)] [[PubMed](#)]
38. Wasag, J.; Grabarczyk, M. Copper film modified glassy carbon electrode and copper film with carbon nanotubes modified screen-printed electrode for the Cd (II) determination. *Materials* **2021**, *14*, 5148. [[CrossRef](#)]
39. Buffon, E.; Stradiotto, N.R. A molecularly imprinted polymer on reduced graphene oxide-gold nanoparticles modified screen-printed electrode for selective determination of ferulic acid in orange peels. *Microchem. J.* **2021**, *167*, 106339. [[CrossRef](#)]
40. Mohammadzadeh Jahani, P.; Beitollahi, H.; Di Bartolomeo, A. A voltammetric sensor for the determination of hydroxylamine using a polypyrrole nanotubes-modified electrode. *Appl. Sci.* **2022**, *12*, 7485. [[CrossRef](#)]
41. Torres-Rivero, K.; Florido, A.; Bastos-Arrieta, J. Recent trends in the improvement of the electrochemical response of screen-printed electrodes by their modification with shaped metal nanoparticles. *Sensors* **2021**, *21*, 2596. [[CrossRef](#)] [[PubMed](#)]
42. Kamble, B.; Garadkar, K.M.; Sharma, K.K.; Kamble, P.; Tayade, S.; Ajalkar, B.D. Determination of 4-nitrophenol using MoO<sub>3</sub> loaded glassy carbon electrode via electrochemical sensing approach. *J. Electrochem. Sci. Eng.* **2021**, *11*, 143–159. [[CrossRef](#)]
43. Abrishamkar, M.; Ehsani Tilami, S.; Hosseini Kaldozakh, S. Electrocatalytic oxidation of cefixime at the surface of modified carbon paste electrode with synthesized nano zeolite. *Adv. J. Chem. A* **2020**, *3*, 767–776.
44. Tajik, S.; Beitollahi, H.; Garkani Nejad, F.; Safaei, M.; Mohammadzadeh Jahani, P. Electrochemical sensing of Sudan I using the modified graphite screen-printed electrode. *Int. J. Environ. Anal. Chem.* **2022**, *102*, 1477–1490. [[CrossRef](#)]
45. Azimi, S.; Amiri, M.; Imanzadeh, H.; Bezaatpour, A. Fe<sub>3</sub>O<sub>4</sub>@SiO<sub>2</sub>-NH<sub>2</sub>/CoSB modified carbon paste electrode for simultaneous detection of acetaminophen and chlorpheniramine. *Adv. J. Chem. A* **2021**, *4*, 152–164.
46. Karimi-Maleh, H.; Sheikhsheoie, M.; Sheikhsheoie, I.; Ranjbar, M.; Alizadeh, J.; Maxakato, N.W.; Abbaspourrad, A. A novel electrochemical epinine sensor using amplified CuO nanoparticles and an-hexyl-3-methylimidazolium hexafluorophosphate electrode. *New J. Chem.* **2019**, *43*, 2362–2367. [[CrossRef](#)]
47. Torres-Rivero, K.; Torralba-Cadena, L.; Espriu-Gascon, A.; Casas, I.; Bastos-Arrieta, J.; Florido, A. Strategies for surface modification with Ag-shaped nanoparticles: Electrocatalytic enhancement of screen-printed electrodes for the detection of heavy metals. *Sensors* **2019**, *19*, 4249. [[CrossRef](#)]
48. Baig, N.; Sajid, M.; Saleh, T.A. Recent trends in nanomaterial-modified electrodes for electroanalytical applications. *TrAC Trends Anal. Chem.* **2019**, *111*, 47–61. [[CrossRef](#)]
49. Kazemi, F.; Zamani, H.; Abedi, M.; Ebrahimi, M. Photodegradation of tramadol using  $\alpha$ -Fe<sub>2</sub>O<sub>3</sub> nanoparticles/12-tungstosilicic acid as an efficient photocatalyst in water sample employing box-behnken design. *Chem. Methodol.* **2021**, *5*, 522–533.

50. Srivastava, A.K.; Upadhyay, S.S.; Rawool, C.R.; Punde, N.S.; Rajpurohit, A.S. Voltammetric techniques for the analysis of drugs using nanomaterials based chemically modified electrodes. *Curr. Anal. Chem.* **2019**, *15*, 249–276. [[CrossRef](#)]
51. Karimi-Maleh, H.; Karaman, C.; Karaman, O.; Karimi, F.; Vasseghian, Y.; Fu, L.; Mirabi, A. Nanochemistry approach for the fabrication of Fe and N co-decorated biomass-derived activated carbon frameworks: A promising oxygen reduction reaction electrocatalyst in neutral media. *J. Nanostruct. Chem.* **2022**, *12*, 429–439. [[CrossRef](#)]
52. Mahmoudi-Moghaddam, H.; Tajik, S.; Beitollahi, H. A new electrochemical DNA biosensor based on modified carbon paste electrode using graphene quantum dots and ionic liquid for determination of topotecan. *Microchem. J.* **2019**, *150*, 104085. [[CrossRef](#)]
53. Eissa, S.; Alshehri, N.; Rahman, A.M.A.; Dasouki, M.; Abu-Salah, K.M.; Zourob, M. Electrochemical immunosensors for the detection of survival motor neuron (SMN) protein using different carbon nanomaterials-modified electrodes. *Biosens. Bioelectron.* **2018**, *101*, 282–289. [[CrossRef](#)] [[PubMed](#)]
54. Eren, T.; Atar, N.; Yola, M.L.; Karimi-Maleh, H. A sensitive molecularly imprinted polymer based quartz crystal microbalance nanosensor for selective determination of lovastatin in red yeast rice. *Food Chem.* **2015**, *185*, 430–436. [[CrossRef](#)]
55. Soto, D.; Alzate, M.; Gallego, J.; Orozco, J. Hybrid nanomaterial/catalase-modified electrode for hydrogen peroxide sensing. *J. Electroanal. Chem.* **2021**, *880*, 114826. [[CrossRef](#)]
56. Tajik, S.; Dourandish, Z.; Garkani Nejad, F.; Aghaei Afshar, A.; Beitollahi, H. Voltammetric determination of isoniazid in the presence of acetaminophen utilizing MoS<sub>2</sub>-nanosheet-modified screen-printed electrode. *Micromachines* **2022**, *13*, 369. [[CrossRef](#)]
57. Amini, R.; Asadpour-Zeynali, K. Cauliflower-like NiCo<sub>2</sub>O<sub>4</sub>-Zn/Al layered double hydroxide nanocomposite as an efficient electrochemical sensing platform for selective pyridoxine detection. *Electroanalysis* **2020**, *32*, 1160–1169. [[CrossRef](#)]
58. Saghiri, S.; Ebrahimi, M.; Bozorgmehr, M. Electrochemical amplified sensor with MgO nanoparticle and ionic liquid: A powerful strategy for methyl dopa analysis. *Chem. Methodol.* **1999**, *5*, 234–239.
59. Samanta, S.; Srivastava, R. CuCo<sub>2</sub>O<sub>4</sub> based economical electrochemical sensor for the nanomolar detection of hydrazine and metol. *J. Electroanal. Chem.* **2016**, *777*, 48–57. [[CrossRef](#)]
60. Alavi-Tabari, S.A.; Khalilzadeh, M.A.; Karimi-Maleh, H. Simultaneous determination of doxorubicin and dasatinib as two breast anticancer drugs uses an amplified sensor with ionic liquid and ZnO nanoparticle. *J. Electroanal. Chem.* **2018**, *811*, 84–88. [[CrossRef](#)]
61. Tajik, S.; Askari, M.B.; Ahmadi, S.A.; Garkani Nejad, F.; Dourandish, Z.; Razavi, R.; Di Bartolomeo, A. Electrochemical sensor based on ZnFe<sub>2</sub>O<sub>4</sub>/RGO nanocomposite for ultrasensitive detection of hydrazine in real samples. *Nanomaterials* **2022**, *12*, 491. [[CrossRef](#)] [[PubMed](#)]
62. Xu, J.; Su, D.; Bao, W.; Zhao, Y.; Xie, X.; Wang, G. Rose flower-like NiCo<sub>2</sub>O<sub>4</sub> with hierarchically porous structures for highly reversible lithium storage. *J. Alloys Compd.* **2016**, *684*, 691–698. [[CrossRef](#)]
63. Tajik, S.; Lohrasbi-Nejad, A.; Mohammadzadeh Jahani, P.; Askari, M.B.; Beitollahi, H. Co-detection of vanillin and folic acid using a novel electrochemical sensor of NiFe<sub>2</sub>O<sub>4</sub>/rGO/ILCPE. *J. Mater. Sci. Mater. Electron.* **2022**, *33*, 2020–2030. [[CrossRef](#)]
64. Jang, G.S.; Kim, E.B.; Akhtar, M.S.; Shin, H.S.; Ameen, S. An exploration of 3-methoxypropionitrile chemical sensor based on layered hexagonal NiCo<sub>2</sub>O<sub>4</sub> nanoplates as electrode material. *Ceram. Int.* **2021**, *47*, 15357–15366. [[CrossRef](#)]
65. Yu, Z.; Li, H.; Zhang, X.; Liu, N.; Tan, W.; Zhang, X.; Zhang, L. Facile synthesis of NiCo<sub>2</sub>O<sub>4</sub>@Polyaniline core-shell nanocomposite for sensitive determination of glucose. *Biosens. Bioelectron.* **2016**, *75*, 161–165. [[CrossRef](#)]
66. Tajik, S.; Beitollahi, H.; Ahmadi, S.A.; Askari, M.B.; Di Bartolomeo, A. Screen-printed electrode surface modification with NiCo<sub>2</sub>O<sub>4</sub>/RGO nanocomposite for hydroxylamine detection. *Nanomaterials* **2021**, *11*, 3208. [[CrossRef](#)]
67. Zhang, C.; Geng, X.; Tang, S.; Deng, M.; Du, Y. NiCo<sub>2</sub>O<sub>4</sub>@rGO hybrid nanostructures on Ni foam as high-performance supercapacitor electrodes. *J. Mater. Chem. A* **2017**, *5*, 5912–5919. [[CrossRef](#)]
68. Wang, Q.; O'Hare, D. Recent advances in the synthesis and application of layered double hydroxide (LDH) nanosheets. *Chem. Rev.* **2012**, *112*, 4124–4155. [[CrossRef](#)]
69. Xue, W.D.; Wang, W.J.; Fu, Y.F.; He, D.X.; Zeng, F.Y.; Zhao, R. Rational synthesis of honeycomb-like NiCo<sub>2</sub>O<sub>4</sub>@NiMoO<sub>4</sub> core/shell nanofilm arrays on Ni foam for high-performance supercapacitors. *Mater. Lett.* **2017**, *186*, 34–37. [[CrossRef](#)]
70. Chu, Q.; Wang, W.; Wang, X.; Yang, B.; Liu, X.; Chen, J. Hierarchical NiCo<sub>2</sub>O<sub>4</sub>@nickel-sulfide nanoplate arrays for high-performance supercapacitors. *J. Power Sources* **2015**, *276*, 19–25. [[CrossRef](#)]
71. Li, L.; Peng, S.; Cheah, Y.; The, P.; Wang, J.; Wee, G.; Ko, Y.; Wong, C.; Srinivasan, M. Electrospun porous NiCo<sub>2</sub>O<sub>4</sub> nanotubes as advanced electrodes for electrochemical capacitors. *Chem. Eur. J.* **2013**, *19*, 5892–5898. [[CrossRef](#)] [[PubMed](#)]
72. Liu, S.; An, C.; Chang, X.; Guo, H.; Zang, L.; Wang, Y.; Jiao, L. Optimized core-shell polypyrrole-coated NiCo<sub>2</sub>O<sub>4</sub> nanowires as binder-free electrode for high-energy and durable aqueous asymmetric supercapacitor. *J. Mater. Sci.* **2018**, *53*, 2658–2668. [[CrossRef](#)]
73. Sahin, O.K.Y. Poly (L-cysteine) modified pencil graphite electrode for determination of sunset yellow in food and beverage samples by differential pulse voltammetry. *Int. J. Electrochem. Sci.* **2018**, *13*, 159–174.
74. Ye, X.; Du, Y.; Lu, D.; Wang, C. Fabrication of β-cyclodextrin-coated poly (diallyldimethylammonium chloride)-functionalized graphene composite film modified glassy carbon-rotating disk electrode and its application for simultaneous electrochemical determination colorants of sunset yellow and tartrazine. *Anal. Chim. Acta* **2013**, *779*, 22–34. [[PubMed](#)]
75. Sierra-Rosales, P.; Toledo-Neira, C.; Squella, J.A. Electrochemical determination of food colorants in soft drinks using MWCNT-modified GCEs. *Sens. Actuators B Chem.* **2017**, *240*, 1257–1264. [[CrossRef](#)]

76. Ghoreishi, S.M.; Behpour, M.; Golestaneh, M. Simultaneous determination of sunset yellow and tartrazine in soft drinks using gold nanoparticles carbon paste electrode. *Food Chem.* **2012**, *132*, 637–641. [[CrossRef](#)]
77. Wu, J.H.; Lee, H.L. Determination of sunset yellow and tartrazine in drinks using screen-printed carbon electrodes modified with reduced graphene oxide and NiBTC frameworks. *Microchem. J.* **2020**, *158*, 105133. [[CrossRef](#)]
78. Darabi, R.; Shabani-Nooshabadi, M. NiFe<sub>2</sub>O<sub>4</sub>-rGO/ionic liquid modified carbon paste electrode: An amplified electrochemical sensitive sensor for determination of Sunset Yellow in the presence of Tartrazine and Allura Red. *Food Chem.* **2021**, *339*, 127841. [[CrossRef](#)]
79. Tran, Q.T.; Phung, T.T.; Nguyen, Q.T.; Le, T.G.; Lagrost, C. Highly sensitive and rapid determination of sunset yellow in drinks using a low-cost carbon materialbased electrochemical sensor. *Anal. Bioanal. Chem.* **2019**, *41*, 7539–7549. [[CrossRef](#)]